Chapter 4

Fabrication of Nanofibrous Scaffolds by Electrospinning

Kai Wei and Ick-Soo Kim

Additional information is available at the end of the chapter

http://dx.doi.org/10.5772/57093

1. Introduction

Continuous progress in surgical technologies and biomedical science has allowed tissue or whole-organ transplantation to become potential options to restore native functions such as regeneration of fractured or diseased bones. Unfortunately, the increasing demand for function transplants and the human aspiration for longer living far exceed the available supply of usable donor tissues. Transplantation technology has encountered severe limitations. Therefore, new technologies are needed to reduce this gap in clinical need versus available healthy tissue and organ supplies. In recent years, electrospinning has been employed as a leading technique for generating biomimetic scaffold made of synthetic and natural polymers for tissue engineering. This method can produce electrospun fibers with diameters in the range from several micrometers down to less than 100 nm that have a very high surface area to mass ratio. This kind of thee dimensional, fibrous scaffold with high porosity can closely biomimic that of native extracellular matrix. Thus, facilitate cell attachment, support cell growth and regulate cell differentiation [1, 2].

Silk filament derived from silkworm *Bombyx mori* is a natural protein mainly made of sericin and fibroin proteins, *i.e.*, sericin (the outer coating) and fibroin (the inner brins). The sericin protein is removed by a process called degumming in industry, so that the term silk is commonly improperly used to define only one of its two components, the silk fibroin. Silk fibroin is a typical fibrous protein that has been studied as a scaffold for tissue engineering because of its excellent biocompatible, bioabsorbability and low level of inflammatory potential [3–5]. In recent years regenerated silk fibroin nanofibers have been developed using electrospinning technique for tissue engineering [4, 5].

In tissue engineering *in vitro*, many researches were directed towards the development of novel hybrid nanofibers scaffold using regenerated silk fibroin by electrospinning technique [6–9] in order to improve cell adhesion, proliferation and differentiation behavior. In current

research, various electrospun nanofibers have been devised to prepare biomimetic nanocomposites for potential application in tissue engineering. For instance, Mather *et al.* prepared silica from nanofibers by immersion of the PEI/PVP (poly(ethylene imine)/poly(vinyl pyrrolidone)) nanofibers in silica precursor tetramethylorthosilicate (TMOS) and then calcinations [10]. A simple alternative to create silk/silica composites is to coat silk-based material templates with silica precursors (such as tetraethylorthosilicate (TEOS)) and subsequently heat them at 105 °C for several h, as was demonstrated with cocoon fibers of *Bombyx mori* fibroin silkworms [11]. Furthermore, the silk template can subsequently be removed by calcinations, yielding a porous material in which the pore structure is determined by the silk-based material.

Bioactive ceramics, such as hydroxyapatite (HA) has also been used in many medical applications in orthopedic and dental surgery owing to its osteoconductivity and osteophilicity [12–14]. In the past few years, various electrospun nanocomposite fibers, such as PCL/$CaCO_3$ [15], HA/gelatin [16], silk/HA [17], PLA/HA [18], and triphasic HA/collagen/PCL [19] had been devised and explored for potential bone regeneration applications. However, since most of these electrospun composite fibers were prepared by electrospinning of blends made by simply mixing the prior obtained inorganic nanoparticles with viscous spinning solutions of polymers, it usually results in nanocomposites with very limited or lacking of specific interactions between the organic and inorganic phases [20].

Besides the widely recognized merits of electrospun fibers, Core-sheath structural nanofibrous scaffold incorporated with bioactive agents is supposed to promote cell migration, proliferation, and gene expressions because the controllable and sustainable release of bioactive agents from the fibers and the preservation of bioactivity. A functional nanofibrous scaffolds incorporated with bioactive agents depends on two factors: the controllable and sustainable release of bioactive agents from the fibers and the preservation of bioactivity. A majority of the reported works on drug release scaffolds tends to adopt the route of simple mixing of bioactive agents and the carrier polymers for blend-electrospinning. The resultant blend formulation would usually lead to initial burst release of drug, which is undesirable for an effective and controllable device. [11] Moreover, simple blending of electrospinning dopes leads to the direct exposure of bioactive agent to aggressive solvent environment that potentially denatures the biomolecules and loses the bioactivity. Therefore, developing novel processes capable of providing controllable system for the release of biomolecules from the electrospun fibers while preserving the bioactivity is of great importance.

In this study, three kinds of nanocomposite scaffold were prepared by electrospinning for improving cell cultivation. Firstly, we describe the formation of regenerated silk fibroin/tetramethoxysilane (TMOS) nanofibers hybrid nanocomposites obtained by electrospinning of their blends. Hydrolysis and condensation of alkoxy silicon monomer (TMOS) shows that the Si–O–Si bonds join together in order to form a network made of porosities. Moreover, the amine groups catalyze the hydrolysis process due to the alternating presence of protonated and non-protonated amine groups in the fibroin molecular chains, which allows hydrogen bond formation with the oxygen adjacent to silicon in the precursor and thus facilitate –Si–O–Si– bond formation [21]. Here we hypothesize that the hybrid of silk fibroin and TMOS could improve hydrophilicity of the fibrous nanocomposites, furthermore, it would improve cell

activity by accelerating adhesion behavior in the early stages. Secondly, a silk-nHA (nano-hydroxyapatite) biocomposite scaffold was also developed by an electrospinning technique and then post-treated by employing a calcium phosphate (Ca–P) alternate soaking method. We hypothesized that well-distributed HA nanoparticles on the silk nanofibrous would improve cell activity by accelerating differentiation in the late stages. Extensive material characterizations and cell culture studies using MC3T3-E1 were conducted to assess the viability and potential application of this material for future bone grafts applications. Furthermore, we present a novel and effective emulsion electrospinning method in obtaining Fluorescein isothiocyanate-dextran (FITC-dextran)/poly (lactic-co-glycolic acid) (PLGA) and Type I collagen/poly (lactic-co-glycolic acid) (PLGA) fibrous composite scaffolds. Core-sheath structured fibers are successfully fabricated with average diameters of 665 nm and 567 nm for FITC-dextran/PLGA and collagen/PLGA, respectively. *In vitro* release profile shows sustained release of encapsulated FITC-dextran from FITC-dextran/PLGA fibers as long as 7 weeks. The osteoblastic activities of collagen/PLGA nanofibrous scaffold are also investigated by employing osteoblastic-like MC3T3-E1 cell line. Lactate dehydrogenase assay results suggest the excellent cytocompatibility. Cell proliferation and alkaline phosphatase (ALP) activity is also ameliorated on this emulsion electrospun collagen/PLGA fibrous scaffold. All the results indicated that this composited scaffold could support the early stages of osteoblast behavior as well as immediate/late stages. The emulsion electrospinning process has good potential for application in drug release device and three-dimensional scaffold in bone regeneration.

2. Fabrication of silk/TMOS composite nanofibers by co-electrospinning

In the electrospinning system [22, 23], a high-voltage power supply (Har-100*12, Matsusada Co., Tokyo, Japan), capable of generating voltages up to 100 kV, was used as the source of the electric field. The regenerated silk protein solution was contained in a plastic tube connected with a capillary tip with an inner diameter of 0.6 mm. The copper wire connected to a positive electrode (anode) was inserted into the polymer solution, and a negative electrode (cathode) was attached to a metallic collector. The solution volume was controlled to keep proper flow rate for spinning.

Silkworm Bombyx mori is a natural protein that is mainly made of sericin and fibroin proteins, *i.e.*, sericin (the outer coating) and fibroin (the inner brins). The sericin protein is removed by a process called degumming in industry, so that the term silk is commonly improperly used to define only one of its two components. In this work, the cocoons of Bombyx mori were degummed three times in an aqueous Na_2CO_3 (0.02 M) at 100 °C for 30 min and washed with distilled water in order to remove sericin from the surface of silk fibers and then the silk fibroin was obtained. The silk fibroin was then dissolved in a ternary solvent system of $CaCl_2$/CH_3CH_2OH/H_2O in 1:2:8 molar ratio at 70 °C with vigorous stirring. After dialysis against distilled water with cellulose tubular membrane with molecular weight cutoffs (MWCO) ranging from 12,000 to 16,000 Daltons for 4 days at 25 °C, the regenerated silk fibroin sponge was obtained by lyophilization (−20 °C, 24 h). the solutions were prepared by dissolving 8% (w/w) regenerated silk protein in 1,1,1,3,3,3-Hexafluoro-2-propanol (HFIP), after 24 h stirring,

5% and 15% (on the weight of silk fibroin) of TMOS was added to the fibroin solution within 30mins under stirring [24–26].

2.1. Morphology of silk/TMOS nanocomposites scaffolds

Electrospun nanofibers of regenerated silk fibroin and its blends with TMOS from their HFIP solutions were obtained using conditions specified above. Figure 1(a) shows SEM image of pure regenerated silk fibroin nanofibers electrospun from a regenerated silk solution dissolved in HFIP at a concentration of 8 wt %. SEM analysis indicates a broad diameter distribution, with an average diameter of 1252 nm and standard deviation (SD) of 410 nm.

The silk/TMOS nanofibers, shown in Figure 1(b, c), were obtained by adding 5 wt % TMOS in 8 wt % regenerated silk fibroin solution within 30 mins under stirring, electrospinning at a voltage of 16 kV and a TCD of 10 cm, and finally drying at 25 °C for 24 h under humidity of 20%. Interestingly, the adjacent fibers in silk/TMOS hybrid electrospun nanofibers caused to 'weld' at fiber contact points [27], as evident in the SEM images (Figure 1(b)). Compared to welded hybrid fibers, the pure silk nanofibers shown in Figure 1(a) are intact and do not show flash welding. Additionally, the fiber diameters showed almost same to 1,287 nm (SD = 367 nm) (Figure 1(b)), to fibers spun from the pure silk solution (Figure 1(a)). The observed 'weld' at contact points may be due to the equilibrium water content, as was verified by TGA analysis shown later. Moreover, as the TMOS concentration increased to 15%, the fibers became belts and the juncture extended like a sheet which could not be identified as nanofiber mats at all (Figure 1(c)). So in this study we just investigated the hybrid nanofibers with the TMOS concentration of 5%.

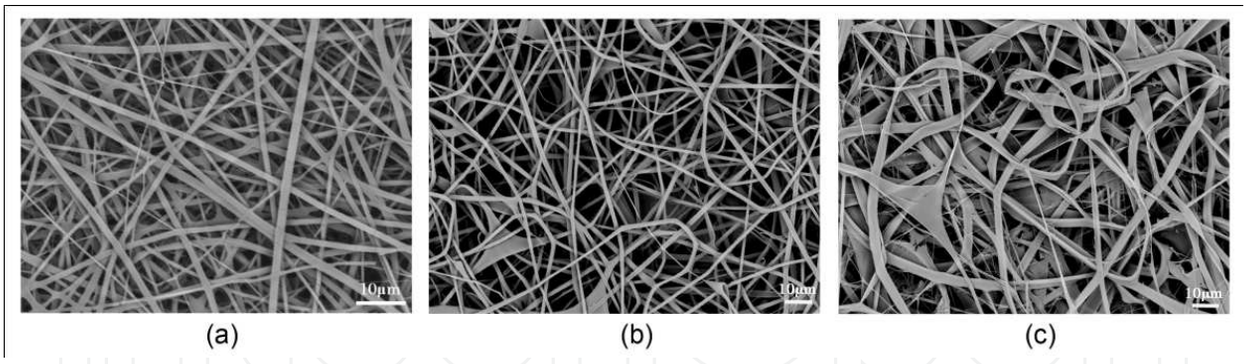

Figure 1. SEM images of the nanofibers (a) regenerated silk fibroin nanofibers; (b) silk/TMOS hybrid nanofibers with TMOS concentration of 5 wt %; and (c) silk/TMOS hybrid nanofibers with TMOS concentration of 15 wt %.

2.2. Hydrophilicity properties of electrospun regenerated silk/TMOS nanofibers

The hydrophilicity of electrospun nanofibers composites can be seen from Figure 2. Water contact angle showed a sharp decrease of electrospun silk nanofibers incorporated with TMOS than pure regenerated silk fibroin nanofiber from 116.2° to 84.8°. Although silk fibroin has many hydrophilic groups such as –OH and –COOH, the incorporation of TMOS result in higher water capacity in the fibers due to the formation of spatial net structure formed *via* Si–

O–Si– linkages as proved by TG result. Furthermore, the water contact of silk/TMOS hybrid nanocomposites was closed to that of TCD (Tissue culture Dish) template (75.6°), which indicated that it may be more suitable for cell attachment than pure silk nanofibers because the optimum water contact of the surface for fibroblast adhesion is reported in the range between 55° and 75° [28]. The adhesion behavior will be discussed in the following text.

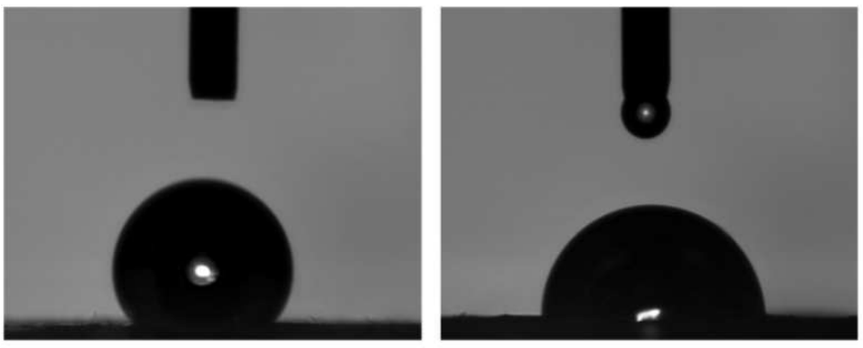

Figure 2. Water contact angle of (a) pure silk nanofibers; and (b) silk/TMOS nanofibers.

2.3. Cytotoxicity assay

Lactate dehydrogenase (LDH) leakage assay results in Figure 3(a) suggest that cell culturing on silk/TMOS fibrous scaffolds cause LDH release near 8% while that on silk is near 7%. Both of them are of no significant difference with the LDH release from TCD as a control. The results showed that the incorporation of TMOS in the fibrous material didn't affect the excellent biocompatibility of silk fibroin. From the live/dead fluorescence micrographs in Figure 3(b) and (c), the majority of cells incubated for 12 h on silk/TMOS and silk scaffolds were alive and parts of them revealed spindle shaped morphology. Cytotoxicity assays indicate that L929 cells on silk/TMOS fibrous scaffold have comparable viability on silk fibrous scaffold.

2.4. Adhesion behavior of electrospun regenerated silk/TMOS nanofibers

The adhesion ratio of L929 cells on pure silk, silk/TMOS nanofibers and TCD controls were shown in Figure 4(a). The cell adhesion ratio of silk/TMOS nanofibers was significantly higher than pure silk nanofibers and TCD controls in all the culture times, it reached as high as 95% after 90 mins' cultivation while that on pure silk was near 85%. Although an increase in adhesion ratio on both pure silk nanofibers and TCD controls after 30 to 90 mins of cell culture were observed, results of adhesion ratio of silk/TMOS nanofibers showed excellent attachment behavior to L929 cells which could be attributed to the melioration of hydrophilicity. The incorporation of TMOS on silk fibroin nanofibers had enhanced the adhesion behavior of L929 cells as expected.

Immunofluorescence microscopy of L929 cells grown on pure silk, silk/TMOS fibrous scaffold and TCD after 6 h cultivation are shown in Figure 4(b-d). Blue fluorescence of cell nuclei

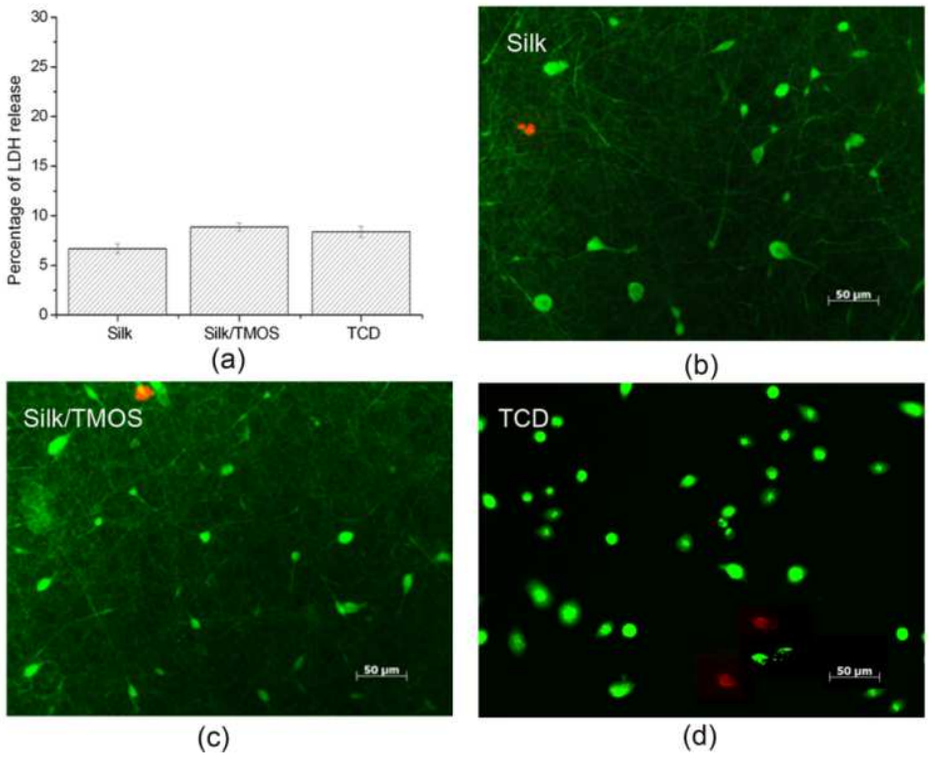

Figure 3. LDH release (a) and fluorescence micrographs of Calcein AM/PI-stained L929 cells with live cells fluorescing green and dead cells fluorescing red after 12 h culture on the Silk/TMOS; (b), silk; (c) nanofibrous scaffold; and TCD (d).

revealed round, well-spaced, and regularly distributed nuclei across the surface of both fibrous scaffolds. Compared to the L929 cells on pure silk that showed round shaped, the cytoskeletal organization (green fluorescence) of most cells on silk/TMOS scaffold showed obvious spindle-shaped morphology, while both round and spindle-shaped L929 cells have been investigated on TCD as a control. Moreover, only L929 cells on silk/TMOS showed vinculin signals (red fluorescence) at the extremities of cellular extensions. Consisting with the adhesion ration in Figure 4 (a), these results mean a better adhesion and stretching behavior of L929 cells on silk/TMOS nanofibrous scaffold than that on pure silk scaffold.

Accordingly, intensive researches have been carried out in order to manipulate cellular behavior by modifying the relative properties of materials. Y. Sasai *et al.* induce durable hydrophilicity on the hydrophobic of polystyrene surface and further modified it by RGD sequence which can be recognized by the receptor protein on the cellular membrane to enhance the adhesion and proliferation of PC12 cell [29]. Vera A. *et al.* induced stable cell adhesion by manipulating the surface topography to the hydrogel poly (ethylene glycol) although fibroblast is intrinsically non-adhesive to the smooth surface [30]. Mohammad *et al.* found that the positive surface of the titanium cylinder results in favorable NCTC clone 929 fibroblast cell adhesion [31]. The results in our study suggested that the cell adhesion ratio and spreading on silk/TMOS has been enhanced comparing to the pure silk. This can be explained by the change of fibrous surface properties in the terms of hydrophilicity and surface morphology change. First of all, water contact angle showed that silk/TMOS have better hydrophilicity than

http://dx.doi.org/10.5772/57093

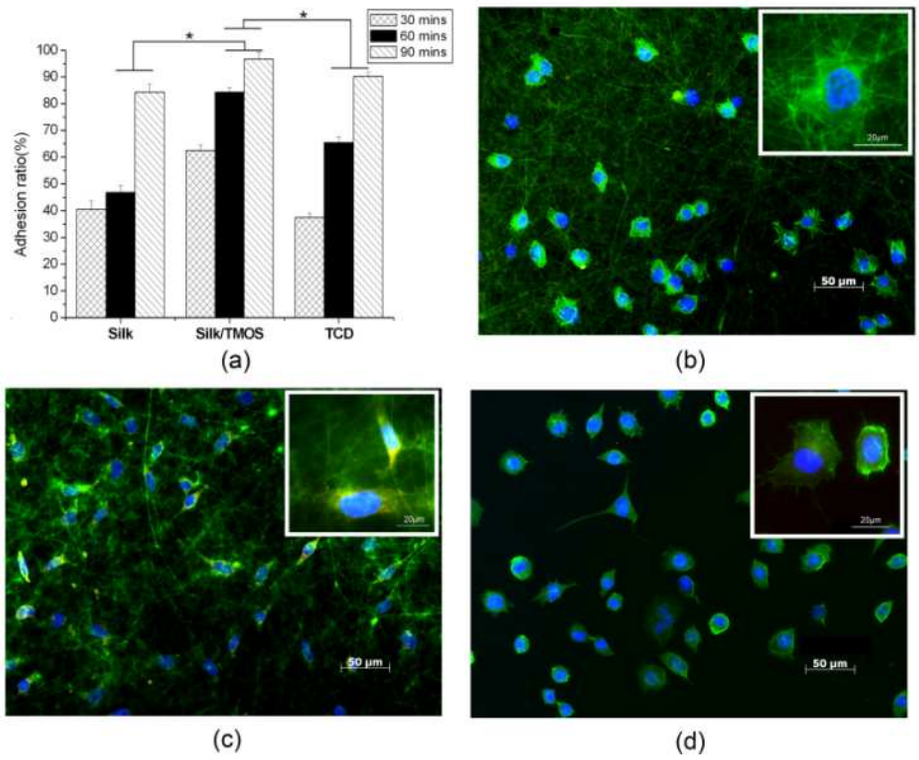

Figure 4. The adhesion ratio (a) for L929 cells after 90 min culture on pure silk, silk/TMOS nanofibers and TCD controls. Significant difference between different materials groups were denoted as * ($p < 0.05$). and Fluorescent staining of F-actin (green), vinculin (red), and cell nuclei (blue) for L929 cells after 6 hs culture on silk; (b) fibrous scaffold, silk/TMOS; (c); and TCD (d).

neat silk because of the formation of spatial net structure formed *via* Si–O–Si– linkages. Studies about the wettability, initial protein adsorption, and the cell adhesion showed that one of the fibronectin state has more active conformation (secondary structure rearrangements) being on a hydrophilic surface [32, 33]. This will consequently lead to more spreading of fibroblasts and ultimately the sufficient cell adhesion and spreading. It has been reported that the optimum wettability of the surface for fibroblast adhesion is in the range between 55° and 75° [28]. The TCD used in this study as control has a water contact of 75.6° (data not shown) and the incorporation of TMOS has change the hydrophobic silk surface of 116.2° to hydrophilic 84.8°. Secondly, SEM images in Figure 1(b, c) showed the interesting adjacent fibers in silk/TMOS hybrid electrospun nanofibers caused to 'weld' at contact points. It has been known that the substrate's topography has a great influence on the behavior of cells at interface. Studies showed that contact guidance happened to cells of different types on different materials with different sizes and shapes of patterns [34–36]. Probably, this kind of 'weld' in silk/TMOS nanofibrous mats influence the surface microstructure of the fiber that might has positive effect to the L929 cell adhesion, though more intensive study is necessary for the conclusion. Nevertheless, considering the complexity of cell surface interaction, which involves protein absorption and specific binding, the function groups that existed in TMOS and net charges presented on the silk/TMOS hybrid scaffold might also influence the protein adsorption and therefore cell adhesion in some degree [37, 38].

3. Fabrication of silk/nHA composite nanofibers

The regenerated silk fibroin sponge was obtained using the same method as described above. Silk fibroin solutions in the concentration of 18% (w/w) were prepared by dissolving the regenerated silk protein sponge into 98% formic acid, and used for electrospinning [39]. The electrospun silk nanofiber was post-treated by a Calcium–Phosphate (Ca–P) alternate soaking method. That is, mineralization of nHA was achieved by subjecting the nanofibers in a series of calcium and phosphate treatments, deemed as the alternate soaking method [40]. Silk nanofibrous scaffolds were first immersed in 0.5 M of $CaCl_2$ (pH of 7.2) (Aldrich Chemical Company, Inc., St. Louis, State Abbreviation, USA), followed by rinsing with deionized (DI) water. Afterwards, the scaffolds were subsequently immersed in 0.3 M of Na_2HPO_4 (pH of 8.96) (Merck & Co. Inc., City, NJ, USA) and rinsed with DI water. The above-mentioned step was referred to as 1 cycle of Ca–P treatment. All nanofibers were subjected to 3 cycles of Ca–P treatments, where the first cycle was 10 min (in each chemical solution) and the second and third cycles were 5 min (in each chemical solution). After mineralization, the nanofibers were freeze-dried overnight.

3.1. Morphology of silk/nHA nanofibrous scaffolds

Mineralization of nHA was successfully deposited on pure silk fibroin nanofibers after 3 cycles [41] of Ca–P treatment as depicted in Figure 7. As shown in Figure 5(b,c), the diameter of obtained silk fibroin nanofibers was around 242 ± 34 nm. It was observed that nHA was homogenously formed on pure silk nanofiber substrates. As evidenced in the high resolution FE-SEM micrograph (Figure 5(d)), nHA particles formed on silk fibroin nanofibrous scaffolds were nanocrystalline in structure and the deposition was occurred predominately on the surfaces of the nanofibrous scaffolds. The size of nHA particles was approximately 30–35 nm in diameter, which was proved by WAXD (see below).

3.2. Crystal Structure of Silk/nHA Nanofibrous Scaffolds

XRD results as can be seen in Figure 8 clearly demonstrated the presence of nHA in the mineralized silk/nHA nanofibrous scaffolds (Figure 6(b): nHA residues and Figure 6(c): mineralized silk/nHA nanofibers). The broad halo peak at 20.6° in Figure 6(c) was attributed to the silk II form of β-sheet crystalline structure [42, 43]. All the peaks in Figures 6(b) and (c) were consistent with the peaks associated with pure nHA (Figure 6(a)), suggesting that rapid mineralization approach used in our study was effective in producing nHA phases on the silk nanofibrous substrates. But unfortunately, both the EDX and XRD analyses indicate the poor crystallinity of the nHA formed on silk nanofibers. It can be explained that the hydroxyl or amide group, which existed in the silk fibroin macro chains, captured calcium or phosphate ions in the solution by chelation. The supply of calcium or phosphate ions to the apatite nuclei was retarded, and the apatite crystals grew under the condition that the calcium or phosphate ions were not sufficiently supplied. Therefore, the crystal growth of apatite was inhibited along a particular axis and resulted in random orientations of crystals in the mineralized fibroin [44].

http://dx.doi.org/10.5772/57093

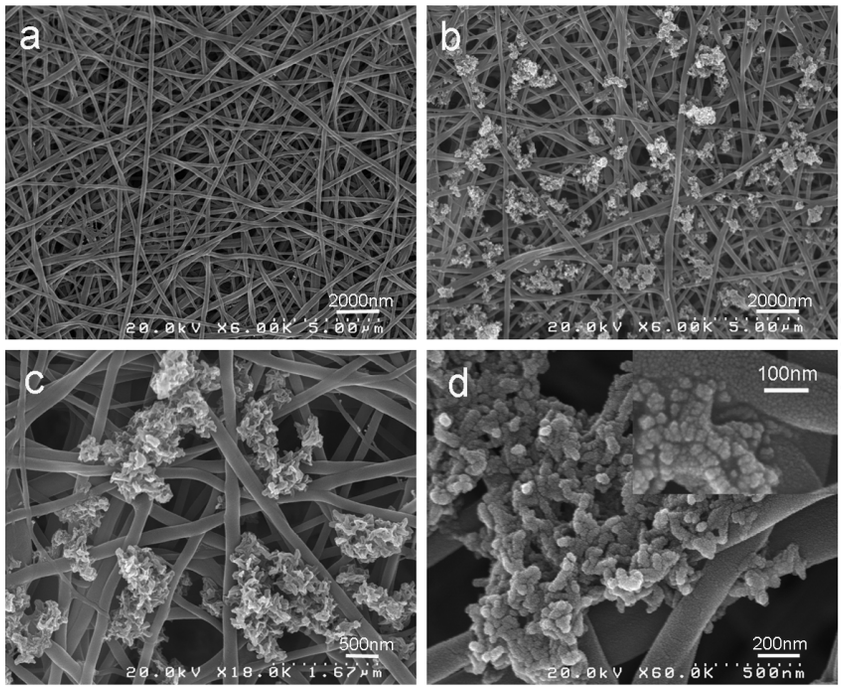

Figure 5. FE-SEM images of pure silk and mineralized silk/nHA nanofibers after 3 cycles of Ca–P treatment. (a) pure silk nanofibers (6000 ×; scale bar, 500 nm), (b–d) mineralized silk/nHA nanofibers after 3 cycles of Ca–P treatment with different magnification.

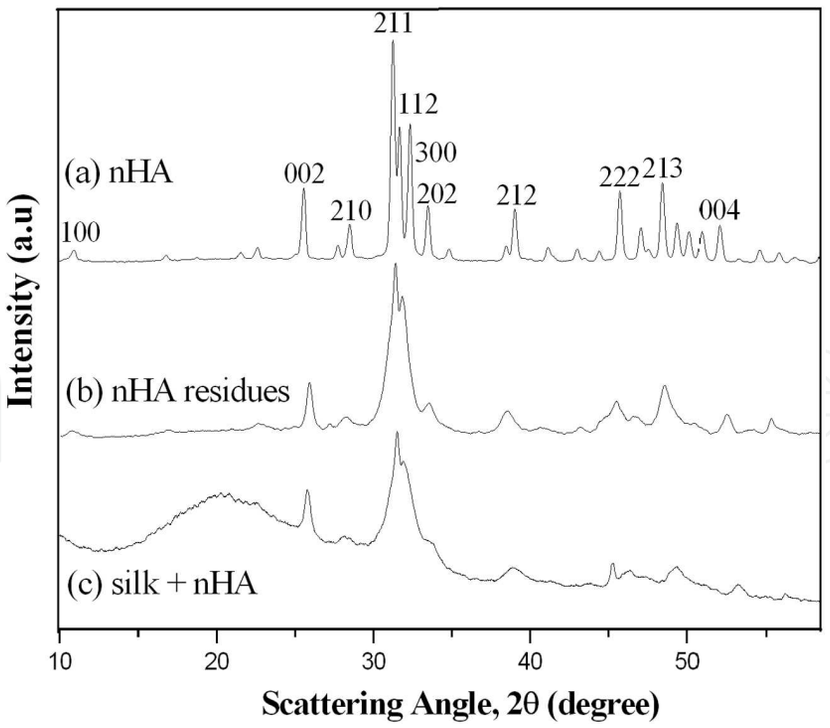

Figure 6. X-ray diffraction (XRD) patterns of (a) pure HA (control); (b) nHA residues; and (c) mineralized silk/nHA nanofibers.

3.3. Proliferation behavior of silk/nHA nanofibrous scaffolds

In Figure 7, immunofluorescence of actin filaments demonstrates the cytoskeletal organization (green). Since the high surface area to volume of nanofibers which is used to mimic the extracellular matrix environment of cells, the MC3T3-E1 cells in Figure 7(I) is investigated to spread in spindle or polygonal morphology after 24 h cultivation. Moreover, intensive vinculin signals can be found along the stretching cellular axis. The MC3T3-E1 cell's adhesion activity in Figure 7(I) suggested that the mineralization of nHA on silk fibrous mats didn't outweigh the benefit of silk nanofibrous scaffold. 3D network culturing morphology of MC3T3-E1 in Figure 7(II) was determined by laser depth-of-focus scanning about 20μm of the silk-nHA scaffold. Together with the cross-section image of Figure 7(III) where a portion of cells are penetrated into fabricated channels, silk-nHA fibrous mats were proved to be suitable for supporting the MC3T3-E1's 3D cultivation.

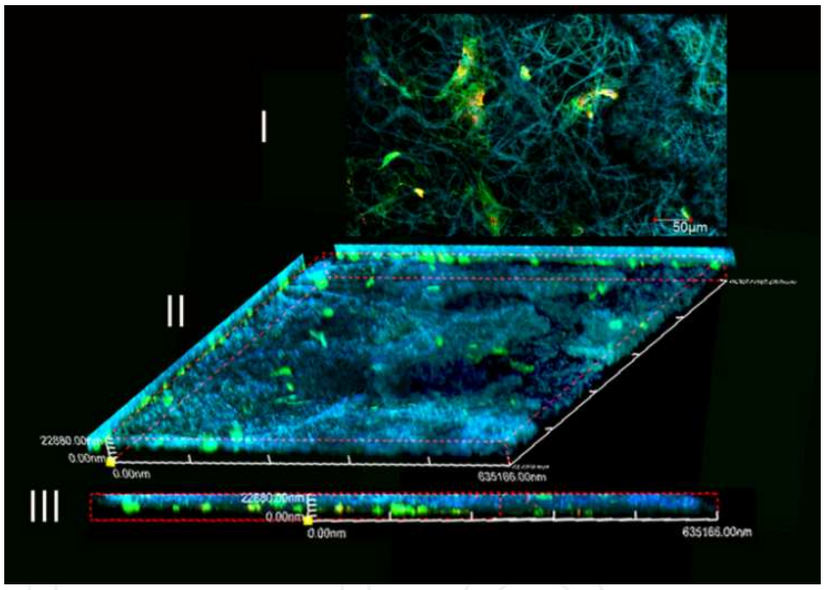

Figure 7. Fluorescent staining of F-actin (green), vinculin (red), and cell nuclei (blue) for MC3T3-E1 cells after 24 h cultivation on silk/nHA fibrous scaffold. (I) 2D morphology of cultivation; (II) 3D morphology by laser scanning of fibrous scaffold; and (III) cross section of II.

As evidenced in the FE-SEM micrographs, osteoblasts were successfully seeded on both pure and mineralized silk nanofibers where the cells were partly adhered to nHA regions in the silk/nHA nanofibers (Figure 8(b)). The deposition of nHA did not affected the MC3T3-E1 attachment compared to those on those grown on pure silk nanofibers after 1 day cultivation (Figures 8(a) and 8(b)) [45, 46], Likewise, cell spreading in a spindle-like shape was also observed on HA-based composites after 2 days of cell culture due to the physical contacts between cells which is maintained *via* the formation of filopodia or lamellipodia [47]. As seen in Figure 8(d), the cells were strongly anchored on the silk/nHA nanofibrous scaffolds, with

http://dx.doi.org/10.5772/57093

preferential attachment of the pseudopodia to nHA regions. In addition, a greater cell spreading on silk/nHA nanofibers was observed after 2 days of cell culture (Figure 8(d)), compared to that after 1 day (Figure 8(b)). When the culture period is prolonged in our study, full cell coverage was found on the nanofibers, and eventually osteoblasts covered most of the nanofiber surfaces after 7 days of cell culture with extended lamellipodia, creating a cell multi-layers on the fibers (Figure 8(f)).

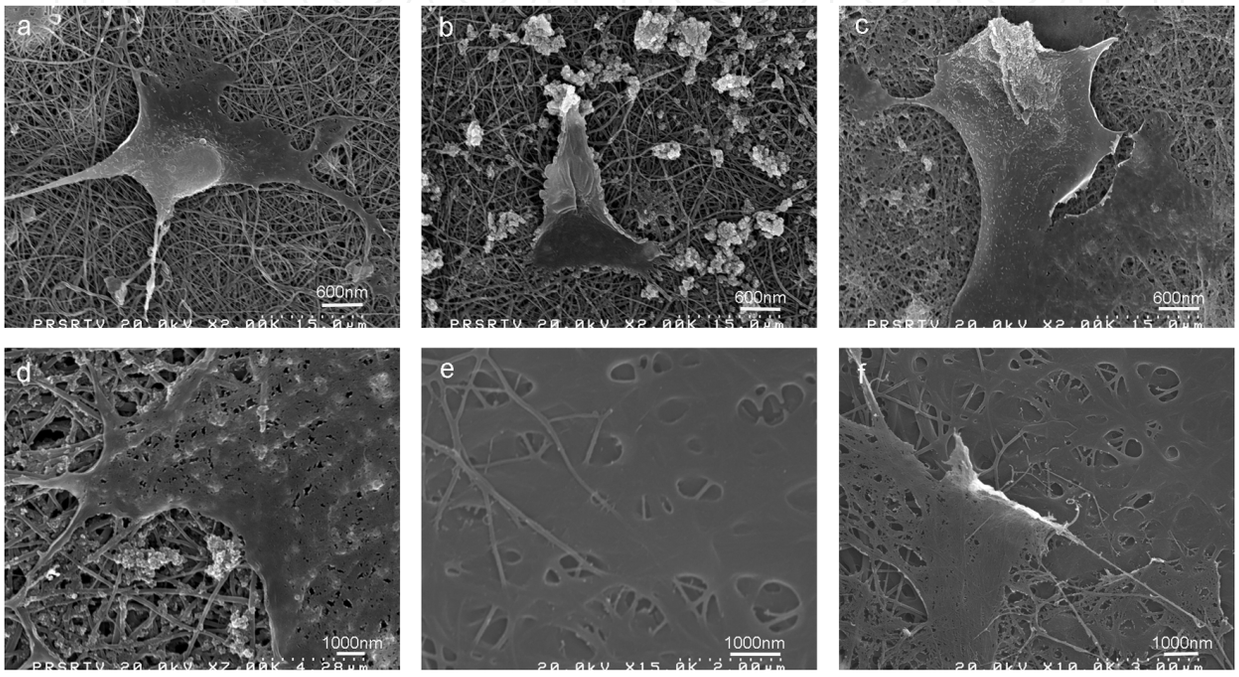

Figure 8. Osteoblasts on pure and mineralized silk/nHA nanofibers. (a) pure silk (day 1); (b) silk/nHA (day 1); (c) pure silk (day 2); (d) silk/nHA (day 2); (e) pure silk (day 7); and (f) silk/nHA (day 7).

Figure 9 shows cell proliferation on pure and mineralized silk nanofibers onward 3 days of cultivation. It was observed that when compared with the pure silk nanofibers, the cell numbers were smaller for mineralized silk/nHA nanofiber scaffold and TCD until 7 days cultivation. This is different from what was observed in other studies where osteoblast proliferation was improved on nanophase HA materials [48, 49]. Probably, the difference was due to the size effect of hydroxyapatite nanoparticles on proliferation as well as the density or bulk distribution. Moreover, previous studies showed that curved nHA surface at a nanometer level could decrease osteoblast-like cells on early period of proliferation [50]. The previously reported results [51–53] were also coincided with those observed in our study: surface topography had a crucial influence on cell behavior, which was accompanied by attenuated proliferation rates on rougher surfaces. Nevertheless, after 14 days of cultivation, cell number on mineralized silk is of no significant differences between pure silk and TCD controls ($p \geq 0.05$), suggesting that the addition of nHA had no negative effect on later period of cell proliferation.

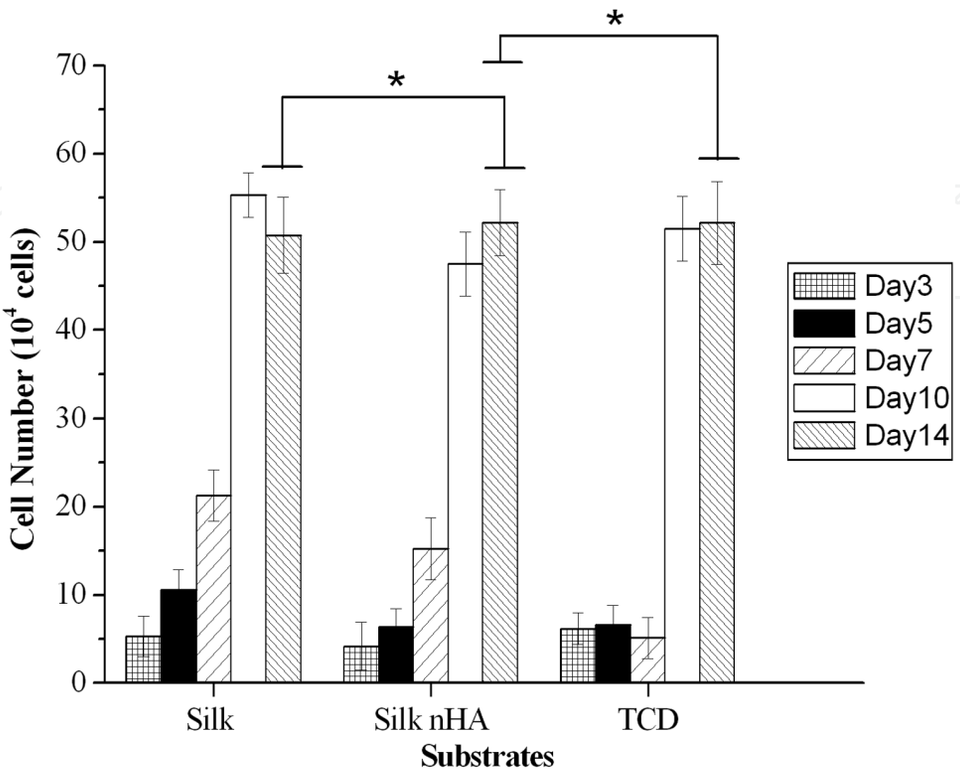

Figure 9. Cell proliferation on pure and mineralized silk nanofibers after 3 to 14 days of cell culture. Significant difference between different materials groups were denoted as * ($p \geq 0.05$).

3.4. Alkaline phosphatase (ALP) activity of silk/nHA nanofibrous scaffolds

One of the properties of nHA is its bioactive nature which promotes osteoblastic differentiation *in vitro* [54–56]. ALP-hydrolyzed phosphate esters play an essential role in the initiation of the cell differentiation process. Thus, ALP activity, as a marker of osteoblastic activity and a standard to evaluate the differentiation of MC3TC-E1 cells, were measured and shown in Figure 10. There was a slight reduction in ALP activity on the pure silk and mineralized silk/nHA nanofibers than TCD after 5 days of cell culture, while a significant increase in ALP activity on both pure silk and mineralized silk/nHA nanofibers after 7 to 14 days of cell culture, compared to TCD counterparts. Results of ALP activity of pure silk and mineralized silk/nHA nanofibers were comparable on an early stage after 5 days of cell culture, but after 7 days of cell culture ALP activity was meliorated in mineralized silk/nHA than pure silk substrates. The incorporation of nHA on silk fibroin nanofibers had enhanced the differentiation activity of MC3T3-E1 from day 7 to 14. After 14 days of cell culture, ALP activity on mineralized silk/nHA nanofibers was nearly 1.6 times higher than that of pure silk nanofibers. One noteworthy observation was that ALP activity in pure silk and mineralized silk/nHA nanofibers was superior to that of TCD as a control from 7 to 14 days of cell culture.

http://dx.doi.org/10.5772/57093

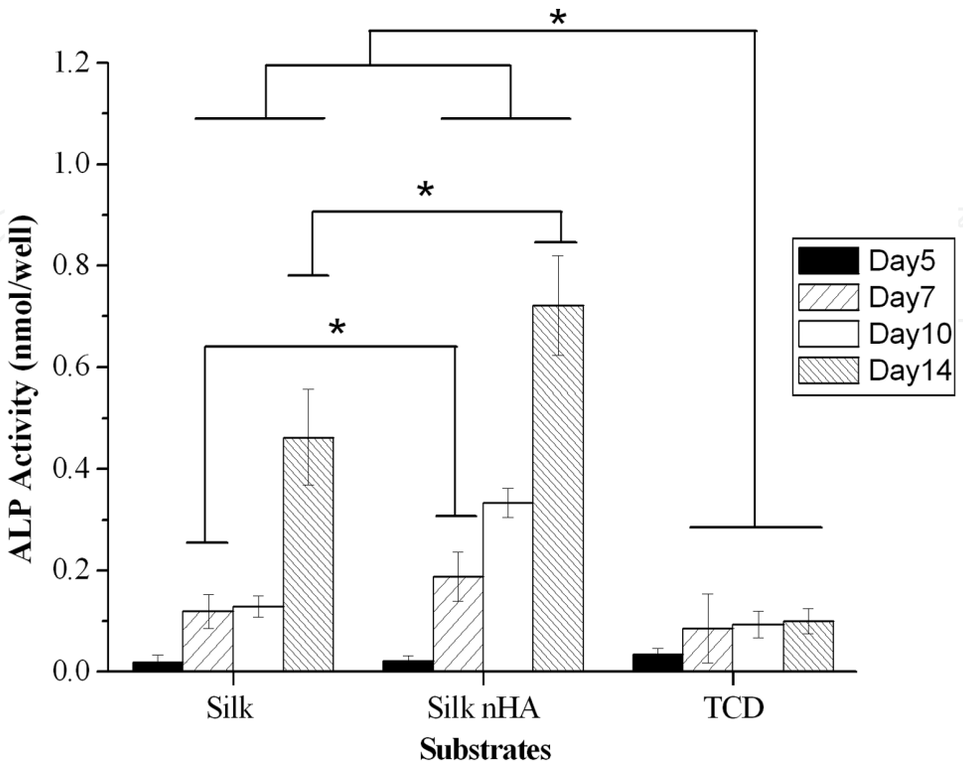

Figure 10. ALP activity on pure and mineralized silk/nHA nanofibers after 5, 7, 10 and 14 days of cell culture. Significant difference between different materials groups were denoted as * ($p < 0.05$).

4. Fabrication of core-sheath structured nanofibers by emulsion electrospinning

There are two possible approaches of incorporating biomolecules in the fibers during electrospinning. These approaches include coaxial electrospinning and emulsion electrospinning. The coaxial electrospinning utilizes two feeding capillary channels for different solutions thus maintaining the functional activity of bimolecular. [57] However, special apparatus is required for coaxial electrospinning and it demands careful adjustment of the operational conditions in order to obtain desirable results. On the other hand, emulsion electrospinning has attracted growing interests, [58-60] due to its relative simplicity and capability of preparing core-sheath type nanofibers using normal solution electrospinning process. In emulsion electrospinning, an aqueous drug solution is prepared and dispersed into a polymer solution in an organic solvent to form a water-in-oil emulsion electrospinning dope. However, the emulsifying process by ultra-sonication might cause conformational changes of biomolecules that affect its bioactivity. Thus, it is necessary not only to prepare emulsion electrospun fibrous scaffold where encapsulated proteins can be controllably released but also to preserve the bioactivities of the encapsulated biomolecules during the emulsifying process.

In this study, poly (lactic-co-glycolic acid) (PLGA), a hydrophilic polymer with excellent biocompatibility and biodegradability which has been widely used in drug delivery and scaffold application, [61-63] was dissolved in chloroform/toluene (C/T) mixed solvent to form the oil phase of the emulsion. SPAN80 (Sorbitan Monooleate) was selected as a non-ionic surfactant widely used in pharmaceuticals and presumed to be non-toxic for biomedical use. The Fol-8Col dissolved in aqueous solution was emulsified with the PLGA oil phase to prepare the emulsion electrospinning dope. (Figure.11) The past work in emulsion electrospinning has been limited to relatively low water content of 4 vol.% (volume percent). [64] For some biomacromolecules that have comparatively low solubility in water, higher water content in the emulsions may be advantageous for their desirable encapsulation in fibers. The concept of using emulsion as a modulator in electrospinning was reported by J.C. Sy *et al*. [65] Here, we propose to introduce emulsions with high water content of 10 wt.% (weight percent). The distribution and inner layer structure of the encapsulated Fol-8Col was investigated. Moreover, release profiles of encapsulated Fol-8Col from the fibrous mats and its short-term cell cytocompatibility to fibroblasts cell line L929 were tested for its potential application as a drug release device as well as tissue engineering scaffold.

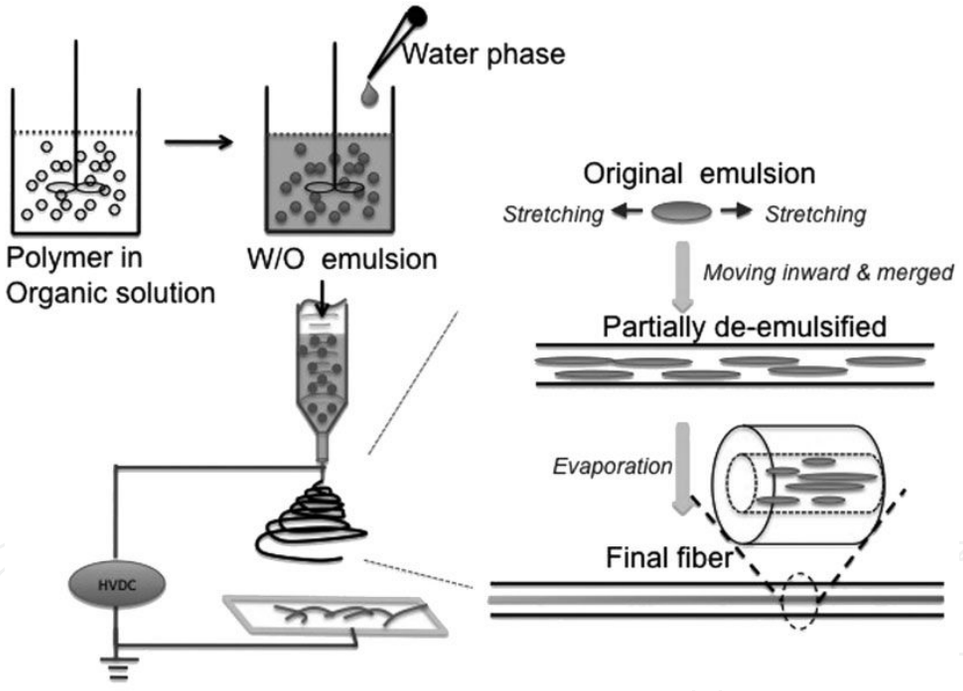

Figure 11. Schematic of emulsion electrospinning.

4.1 Characterization of the encapsulation

In order to clarify the encapsulation of Fol-8Col inside the fibers, two means were employed to characterize the encapsulation effect. FITC produces green fluorescence at 490nm. The

fluorescence micrographs of NHS-Fluorescein labeled Fol-8Col/PLGA showed fluorescence emitting fibers (Figure 12), suggesting the homogeneous presence of Fol-8Col in the emulsion electrospun fibers. Consisting with the SEM images in Figure 1, bead defects of fibrous morphology were not observed.

TEM observation was further conducted to identify the layer structure of emulsion electrospun fibers in this study. The TEM image of Figure 13 suggested that the inner component Fol-8Col of W/O emulsion was properly wrapped in the centre of resultant composite fiber. The boundary in the TEM images reflects the difference of electron transmission ability between the core (Fol-8Col) and sheath (PLGA). However, a slanted portion of boundary can be observed which is associated with the miscibility of amphiphilic surfactant (SPAN80) molecule.

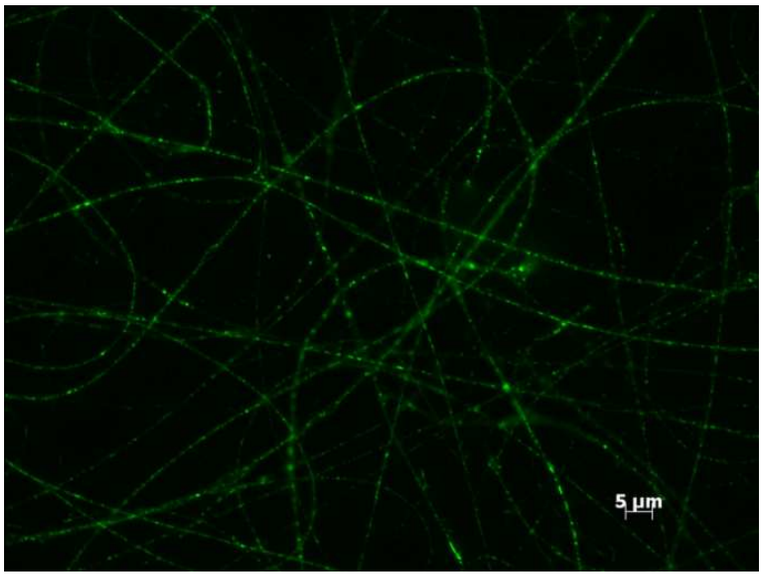

Figure 12. Fluorescence microphotograph of Fol-8Col/PLGA fibers electrospun with Fol-8Col (5 wt% aqueous content), a C/T weight ratio of 75/25, and 10wt% PLGA.

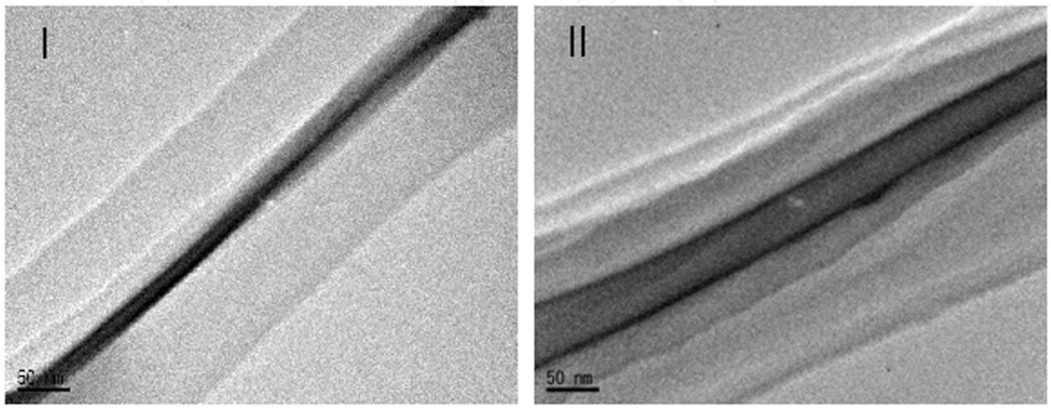

Figure 13. TEM images of Fol-8Col/PLGA fibers electrospun from Fol-8Col [5 (I) and 10wt%(II) aqueous content], with a C/T weight ratio of 75/25 and a PLGA concentration of10 wt%.

4.2 Cytotoxicity assay and live/dead cell staining

The cytocompatibility test of murine fibroblast L929 on Fol-8Col/PLGA emulsion electrospun fibrous scaffold was performed to investigate its potential for tissue engineering application. Here we chose the fibrous scaffold prepared from the electrospinning dope of Fol-8Col aqueous 5 wt.%, PLGA 10 wt.%, C/T 75:25. Collagen/PLGA fibrous mat (morphological data not shown) produced under the same electrospinning condition were tested as control. Figure 14 shows that LDH release after 24 hours' cultivation on all the samples was approximately 10% percent without significant difference ($p>0.05$). From the live/dead fluorescence micrographs, the majority of live cells incubated on Fol-8Col/PLGA scaffold can be observed with stretching spindle shaped morphology. The cytotoxicity assays indicate that the L929 cells have comparable viability on Fol-8Col/PLGA scaffold as that on Collagen/PLGA scaffold.

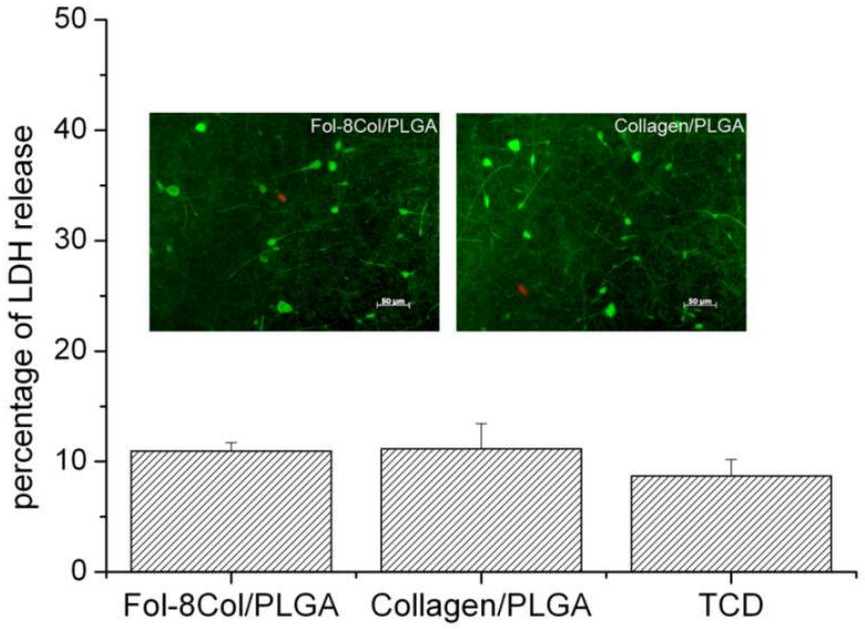

Figure 14. L929 cell LDH leakage results and fluorescence micrographs of Calcein AM/PI-stained L929 cells with live cells fluorescing green and dead cells fluorescing red after 24 h culture on the Fol-8Col/PLGA and collagen/PLGA as a control. Fibers are electrospun at 5 wt% protein aqueous content, C/T 75/25, and 10wt% PLGA.

4.3 Adhesion ratio and cell morphology

The adhesion activity of L929 cells on Fol-8Col/PLGA scaffold is shown in Figure 15. After 6 hours of cultivation, the adhesion ratio of L929 cells on Fol-8Col/PLGA achieved 62±2.3% while that on PLGA is 45±3.4%. This can be attributed to the effect of the Fol-8Col, which is a hydrophilic compared to PLGA molecule; where in the RGD sequences in Fol-8Col molecule has been proven effective at improving cell adhesion. [66] The result shows that the adhesion

http://dx.doi.org/10.5772/57093

ratio (87.6±2.5%) of L929 cells on Fol-8Col/PLGA scaffold after 24 hours cultivation remains higher than that on neat PLGA (68±1.8%).

The immunocytofluorescence staining for nuclei, vinculin, and filamentous actin of L929 cell after 24 hours adhesion shows that L929 cells on both scaffolds exhibited obvious stretching spindle morphology. The filament bundles (green stain) are oriented in a parallel direction following the main cellular axis. A comparatively intensive vinculin signals (red) was investigated on the higher magnificent (630x) image of cells on Fol-8Col/PLGA scaffolds compared to that on PLGA. Our previous results have proved that the biocompatibility of Fol-8Col matrix to L929 cell line is higher than that of the native collagen. [67] The immunocytofluorescence staining results on Fol-8Col/PLGA scaffold in this section is consistent with the adhesion ratio analysis, showing that good cytocompatibility has been preserved after the emulsion electrospinning process.

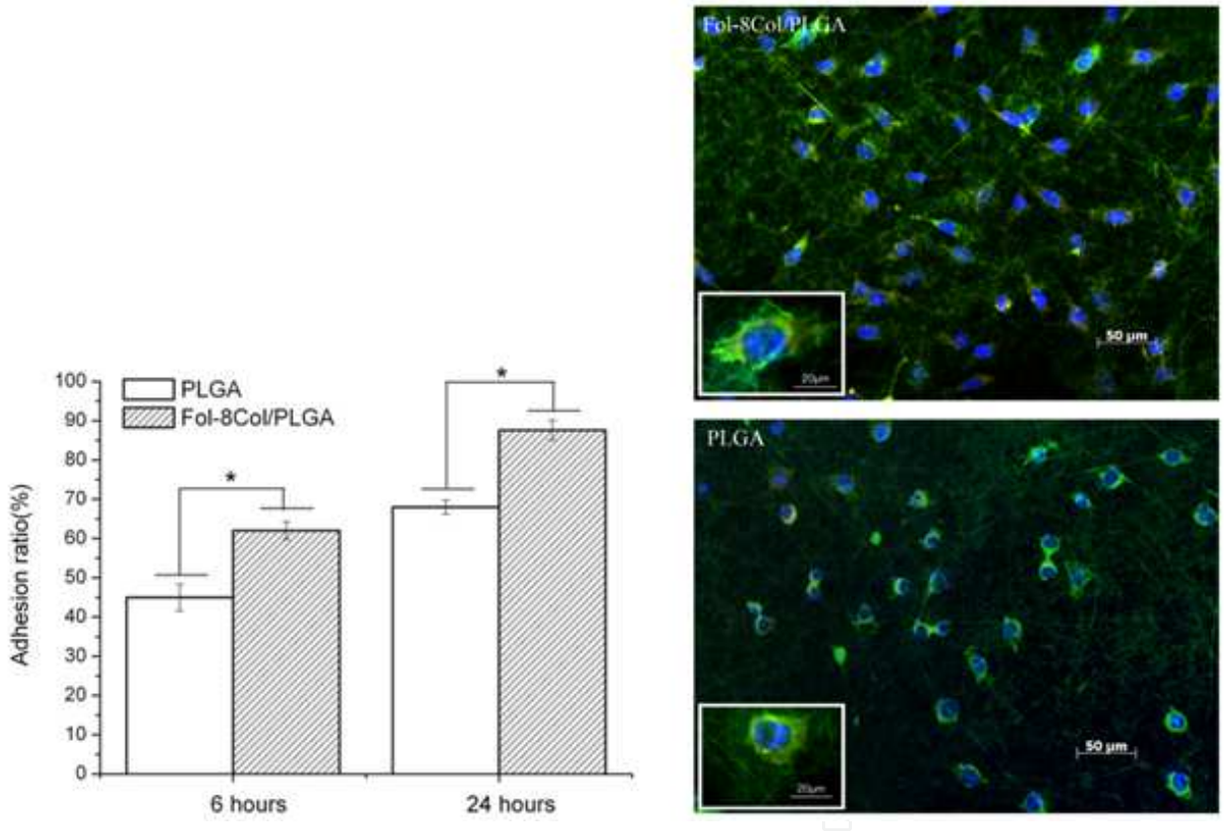

Figure 15. Adhesion ratio and fluorescent staining of F-actin (green), vinculin (red), and cell nuclei (blue) for L929 cells after 24 h culture on a Fol-8Col/PLGA fibrous scaffold (electrospun from 5 wt% Fol-8Col aqueous content, C/T 75/25, and 10wt% PLGA). A neat PLGA fibrous scaffold was used as a control.

Previous studies have addressed the issue of preserving the biomolecular activity through various methods. [68, 69] Our previous research on Fol-8Col has shown that it has excellent biocompatibility to L929 cell line. [4] The results in Figure 14 and 15, show that the cytocompatibility of encapsulated Fol-8Col released from Fol-8Col/PLGA fibrous scaffold to L929 cells were preserved. The effectiveness of SPAN80 in the formation of W/O emulsion is thought to

facilitate the production of core-sheath structure via the electrospinning process. The core-sheath structure lessens the possibility of the exposure of Fol-8Col to the harsh organic solvents and thus protects Fol-8Col from activity loss. We assumed that the collagen derivate sequences, RGD sequences, and the triple-helix have been preserved in Fol-8Col, which is an essential element of its bioactivity.

5. Conclusions

We have successfully prepared three different nanofibrous scaffolds *via* co-electrospinning, post-treatment processes and emulsion electrospinning.

Regenerated silk fibroin/TMOS hybrid nanofibers showed superior fibroblast attachment, compared to pure silk fibroin nanofibers, due to relatively higher hydrophilicity. Accordingly, the silk/TMOS nanofibrous composites showed a sharp decrease in water contact angle than pure regenerated silk fibroin nanofiber due to the spatial net structure formed *via* Si–O–Si– connection which was responsible for water capacity. Interestingly, the electrospinning process caused adjacent fibers to 'weld' at contact points, as confirmed by SEM analysis. This study of simple incorporation silk with TMOS has merit of preserving the excellent biocompatibility of silk, and the fibrous three-dimensional silk/TMOS scaffold can support significantly enhanced L929 adhesion than pure silk. Thus this method might open a new pathway to preparing various functional scaffolds with enhanced bioactivity for in vitro tissue engineering application.

Nano hydroxyapatite was successfully deposited on regenerated silk fibroin nanofibrous scaffolds by a biomimetic Ca–P method. It was found that the primary nHA crystals with a diameter about 30 nm were well-distributed on the surface of the nanofibrous substrates. The ALP expression of the cells was improved on mineralized silk/nHA nanofibers during the cell culture periods, irrespective of the cell number which was leveling off (3 to 7 days). It appeared that the nHA presenting in mineralized silk/nHA nanofibers had a greater improvement on differentiation stages than in an early stage of cultivation, such as adhesion and proliferation. The cell cultivation in this study demonstrated that silk/nHA nanocomposite scaffold could support the early stage of osteoblast adhesion and had a significant effect on the differentiation stage, suggesting that this composite scaffold may be a promising biomaterial for bone tissue engineering.

Furthermore, Fol-8Col, an original designed recombinant collagen-like protein, has been successfully encapsulated in PLGA in the form of core-sheath fibrous structure via emulsion electrospinning. The homogenous encapsulation of the Fol-8Col in a core-sheath form was characterized by the fluorescence micrographs of NHS-Fluorescein labeled Fol-8Col/PLGA and transmission electron microscope. The cytocompatibility of Fol-8Col/PLGA fibers proved its superior ability for L929 cells adhesion compared to that of the neat PLGA. In this regard, this emulsion electrospinning process might open a new pathway to preparing tailored core-sheath fibers to ultimately fulfill the functions of drug release device as well as tissue engineering scaffold.

Acknowledgements

The authors acknowledge the support of Shinshu University Global COE Program "International Center of Excellence on Fiber Engineering".

Author details

Kai Wei* and Ick-Soo Kim

*Address all correspondence to: kim@shinshu-u.ac.jp

Nano Fusion Technology Research Group, Faculty of Textile Science & Technology, Shinshu University, Ueda, Japan

References

[1] Huang, L.; Nagapudi, K.; Apkarian, R.P.; Chaikof, E.L. *J. Biomater Sci. Polym. Ed.* 2001, *12*, 979–993.

[2] Matthews, J.A.; Wnek, G.E.; Simpson, D.G.; Bowlin, G.L. *Biomacromolecules* 2002, *3*, 232–238.

[3] Altman, G.H.; Diaz, F.; Jakuba, C.; Calabro, T.; Horan, R.L.; Chen, J.S.; Lu, H.; Richmond, J.; Kaplan, D.L. *Biomaterials* 2003, *24*, 401–416.

[4] Meinel, L.; Hofmann, S.; Karageorgiou, V.; Kirker-Head, C.; Mccool, J.; Gronowicz, G.; Zichner L.; Langer, R.; Vunjak-Novakovic, G.; Kaplan, D.L. *Biomaterials* 2005, *26*, 147–155.

[5] Panilaitis, B.; Altman, G.H.; Chen, J.S.; Jin, H.J.; Karageorgiou, V.; Kaplan, D.L. *Biomaterials* 2003, *24*, 3079–3085.

[6] Caruso, R.A.; Schattka, J.H.; Greiner, A. *Adv. Mater.* 2001, *13*, 1577–1579.

[7] Hou, H.; Ge, J.J.; Zeng, J.; Li, Q.; Reneker, D.H.; Greiner, A.; Cheng, S.Z.D. *Chem. Mater.* 2005, *17*, 967–973.

[8] Patel, A.C.; Li, S.; Yuan, J.M.; Wei, Y. *Nano Lett.* 2006, *6*, 1042–1046.

[9] Wei, K.; Ohta, T.; Kim, B.S.; Lee, K.H.; Kim, K.W.; Khil, M.S.; Kim, H.Y.; Kim, I.S. *Polym. Adv. Technol.* 2010, *21*, 746–751.

[10] Pritesh, A.P.; Jessica, E.; Maria, C.A.; A. Jon, G.; Patrick, T.M. *Polymer* 2009, *50*, 1214–1222.

[11] Xu, Q.; Li, J.B.; Peng, Q.; Wu, L.L. Li, S.P. *Mater. Sci. Eng. B* 2006, *127*,212–217.

[12] LeGeros, R.Z. Karger: Basel, Switzerland, 1991.

[13] Aoki, H. Tokyo: Ishiyaku Euro America, 1994; 90–130.

[14] Feenstra, L.; de Groot, K. Medical Use of Calcium Phosphate Ceramics. In *Bioceramics of Calcium Phosphate*; de Groot, K, Ed.; CRC Press: Boca Raton, FL, USA, 1982.

[15] Fujihara, K.; Kotaki, M.; Ramakrishna, S. *Biomaterials* 2005, *26*, 4139–4147.

[16] Kim, H.W.; Song, J.H.; Kim, H.E. *Adv. Funct. Mater.* 2005, *15*, 1988–1994.

[17] Li, C.; Vepari, C.; Jin, H.J.; Kim, H.; Kaplan, D.L. *Biomaterials* 2006, *27*, 3115–3124.

[18] Sui, G.; Yang, X.; Mei, F.; Hu, X.; Chen, G.; Deng, X.; Ryu, S. *J. Biomed. Mater. Res. Part A.* 2007, *82A*, 445–454.

[19] Venugopal, J.; Vadgama, P.; Kumar, T.; Ramakrishna, S. *Nanotechnology* 2007, *18*, 055101–055101.

[20] Zhang, Y.; Venugopal, J.R.; El-Turki, A.; Ramakrishna, S.; Su, B.; Lim, C.T. *Biomaterials* 2008, *29*, 4314–4322.

[21] Pohnert, G.; Angewandte, C. *Int. Ed.* 2002, *41*, 3167–3169.

[22] Ohsawa, O.; Lee, K.H.; Kim, B.S.; Lee, S.; Kim, I.S. *Polymer* 2010, *51*, 2007–2012.

[23] Wei, K.; Li, Y.; Kim, K.O.; Nakagawa, Y.; Kim, B.S.; Abe, K.; Chen, G.Q.; Kim, I.S. *J. Biomed. Mater. Res. Part A* 2011, *97*, 272–280.

[24] Zhang, M.; Yi, T.T.; Zhang, Y.M.; Zhang, L.; Wu, W.; Zhang, A.L.; Pan, Z.J. *Polym. Adv. Technol.* 2011, *22*, 151–157.

[25] Yao, C.; Li, X.; Song, T.; Li, Y.; Pu, Y. *Polym. Int.* 2009, *58*, 396–402.

[26] Park, K.E.; Jung, S.Y.; Lee, S.J.; Min, B.M.; Park, W.H. *Int. J. Biol. Macromol., 38*, 165–173.

[27] Li, Y.; Bao. X.X.; Matsuda, N.; Yao, J.M.; Teramoto, A.; Abe, K.; Ko, F.K. *J. Mater. Sci.* 2011, *46*, 1396–1404.

[28] Jang, S.Y.; Seshadri, V.; Khil, M.S.; Kumar, A.; Marquez, M.; Mather, P.T. *Adv. Mater.* 2005, *17*, 2177–2180.

[29] Groth, T.; Altankov, G. *Biomaterials* 1996, *17*, 1227–1234.

[30] Sasai, Y.; Matsuzaki, N.; Kondo, S.; Yamauchi, Y.; Kuzuya, M. *Surf. Coat. Technol.* 2008, *202*, 5724–5727.

[31] Schulte, V.A.; Díez, M.; Möller, M.; Lensen, M.C. *Biomacromolecules* 2009, *10*, 2795–2801.

[32] Hamdan, M.; Blanco, L.; Khaisat, A.; Tresguerres, I.F. *Clin Implant Dent Relat Res.* 2006, *8*, 32–38.

[33] Grinnell, F.; Feld, M.K. *J. Biol. Chem.* 1982, *257*, 4888–4893.

[34] Wei, J.H.; Yoshinari, M.; Takemoto, S.; Hattori, M.; Kawada, E.; Liu, B.L.; Oda, Y.J. *Biomed. Mater. Res.* 2007, *81B*, 66–75.

[35] Lim, J.Y.; Donahue, H.J. *Tissue Eng.* 2007, *13*, 1879–1891.

[36] Curtis, A.; Wilkinson, C. *Biomaterials* 1997, *18*, 1573–1583.

[37] Kidambi, S.; Udpa, N.; Schoeder, S.A.; Findlan, R.; Lee, I.; Chan, C. *Tissue Eng.* 2007, *13*, 2105–2117.

[38] Keselowsky, B.G.; Collard, D.M.; Garcia, A.J. *Biomaterials* 2004, *25*, 5947–5954.

[39] Wang, Y.X.; Robertson, J.L.; Spillman, W.B.; Claus, R.O. *Pharm. Res.* 2004, *21*, 1362–1373.

[40] Wei, K.; Xia, J.H.; Kim, B.S.; Kim, I.S. *J. Polym. Res.* 2010, *18*, 579–585.

[41] Taguchi, T.; Kishida, A.; Akashi, M. *Chem. Lett.* 1998, *8*, 711–712.

[42] Ngiam, M.; Liao, S.; Patil, A.J.; Cheng, Z.; Chan, C.K.; Ramakrishna, S. *Bone* 2009, *45*, 4–16.

[43] Kim, U.J.; Park, J.Y.; Kim, H.J.; Wada, M.; Kaplan, D.L. *Biomaterials* 2005, *26*, 2775–2785.

[44] Furuzono, T.; Taguchi, T.; Kishida, A.; Akashi, M.; Tamada, Y.; Biomed, J. *J. Biomed. Mater. Res.*, 2000, *50*, 344–352.

[45] Zhai, Y.; Cui, F.Z. *J. Cryst. Growth* 2006, *291*, 202–206.

[46] Smith, I.O.; McCabe, L.R.; Baumann, M.J. *Int. J. Nanomed.* 2006, *1*, 189–194.

[47] Itoa, Y.; Hasudaa, H.; Kamitakaharac, M.; Ohtsukic, C.; Taniharac, M.; Kangd, I.K.; Kwon, O.H. *J. Biosci. Bioeng.* 2005, *100*, 43–49.

[48] Ogata, K.; Imazato, S.; Ehara, A.; Ebisu, S.; Kinomoto, Y.; Nakano, T. *J. Biomed. Mater. Res.* 2005, *72*, 127–135.

[49] Liao, S.S.; Cui, F.Z.; Zhu, Y. *J. Bioact. Comp. Poly.* 2004, *19*, 117–130.

[50] Webster, T.J.; Siegel, R.W.; Bizios, R. *Biomaterials* 1999, *20*, 1221–1227.

[51] Zhu, X.; Eibl, O.; Scheideler, L.; Geis-Gerstorfer, J. *J. Biomed. Mater. Res.* 2006, *79*, 114–127.

[52] Bacakova, L.; Stary, V.; Kofronova, O.; Lisa, V. *J. Biomed. Mater. Res.* 2001, *54*, 567–578.

[53] Anselme, K.; Bigerelle, M.; Noel, B.; Dufresne, E.; Judas, D.; Iost, A. *J. Biomed. Mater. Res.* 2000, *49*, 155–166.

[54] Martin, J.Y.; Schwartz, Z.; Hummert, T.W.; Schaub, D.M.; Simpson, J.; Lankford, J. *J. Biomed. Mater. Res.* 1995, *29*, 389–401.

[55] Ayers, R.; Nielsen-Preiss, S.; Ferguson, V.; Gotolli, G.; Moore, J.J.; Kleebe, H.J. *Mater. Sci. Eng. C* 2006, *26*, 1333–1337.

[56] Redey, S.A.; Nardin, M.; Bernache-Assolant, D.; Rey, C.; Delannoy, P.; Sedel, L. *J. Biomed. Mater. Res.* 2000, *50*, 353–364.

[57] Thian, E.S.; Huang, J.; Best, S.M.; Barber, Z.H.; Brooks, R.A.; Rushton, N. *Biomaterials* 2006, *27*, 2692–2698.

[58] Y.Z. Zhang, X. Wang, Y. Feng, J. Li, C.T. Lim, S. Ramakrishna, *Biomacromolecules* 2006, *7*, 1049-1057.

[59] X.L. Xu, X.L. Zhuang, X.S. Chen, X.R. Wang, L.X. Yang, X.B. Jing, *Macromol. Rapid Commun*. 2006, *32*, 1637–1642.

[60] J.F. Zhang, D.Z. Yang, F. Xu, Z.P. Zhang, R.X. Yin, J. Nie, *Macromolecules* 2009, *42*, 5278–5284.

[61] S. Agarwala, A. Greiner, *Polym. Adv. Technol*. 2011, *22*, 372–378.

[62] J. Wang, B.M. Wang, S.P. Schwendeman, *J. Control Release* 2002, *82*, 289–307.

[63] T.B. Bini, S. Gao, T.C. Tan, S. Wang, A. Lim, L.B. Hai, S. Ramakrishna, *Nanotechnology* 2004, *15*, 1459–1464.

[64] H. Pan, H. Jiang, W. Chen, *Biomaterials* 2008, *29*, 1583–1592.

[65] X. Xu, L. Yang, X. Xu, X. Wang, X. Chen, Q. Liang, J. Zeng, X. Jing, *J. Control Release* 2005, *108*, 33–42.

[66] J.C. Sy, A.S. Klemm, V.P. Shastri, *Adv. Mater*. 2009, *21*, 1814–1819.

[67] W. Chen, C.E. Chang, M.K. Gilson, *J. Am. Chem. Soc*. 2006, *128*, 4675–4687.

[68] C. Du, M. Wang, J. Liu, M. Pan, Y. Cai, J. Yao, *Appl. Microbiol. Biotechnol*. 2008, *79*, 195–202.

[69] X. Zong, K. Kwangsok, F. Dufei, R. Shaofeng, B.S. Hsiao, B. Chu, *Polymer* 2002, *43*, 4403–4412.

[70] J. Zeng, A. Aigner, F. Czubayko, T. Kissel, J.H. Wendorff, A. Greiner, *Biomacromolecules* 2005, *6*, 1484–1488.